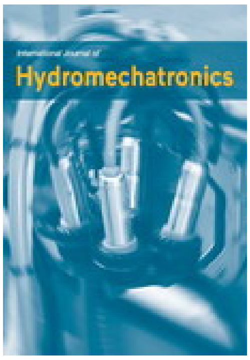

International Journal of Hydromechatronics

ISSN online: 2515-0472 - ISSN print: 2515-0464
https://www.inderscience.com/ijhm

Rolling bearing fault diagnosis based on VMD reconstruction and DCS demodulation

Dong Zhen, Dongkai Li, Guojin Feng, Hao Zhang, Fengshou Gu

DOI: 10.1504/IJHM.2022.10048012

Article History:

Received:	19 January 2022
Last revised:	06 June 2022
Accepted:	22 March 2022
Published online:	25 August 2022

Rolling bearing fault diagnosis based on VMD reconstruction and DCS demodulation

Dong Zhen, Dongkai Li, Guojin Feng* and Hao Zhang

School of Mechanical Engineering,
Hebei University of Technology,
Tianjin 300401, China
Email: d.zhen@hebut.edu.cn
Email: dongk_li@163.com
Email: Guojin.Feng@outlook.com
Email: zhanghao@hebut.edu.cn
*Corresponding author

Fengshou Gu

Centre for Efficiency and Performance Engineering,
University of Huddersfield, UK
Email: f.gu@hud.ac.uk

Abstract: As a major component of rotating machinery, rolling bearings are prone to failure because they usually work in harsh environment and are subjected to heavy cyclic loads. Meanwhile, the fault characteristics of bearings are easily submerged by noise and difficult to extract. To solve this problem, a fault diagnosis method based on variational mode decomposition (VMD) and degree of cyclostationarity (DCS) demodulation is proposed. First, the sparsity-based reconstruction factor can distinguish the sensitivity of VMD modes, and it is used to reconstruct all VMD modes to denoise the signal. Secondly, taking the advantage that DCS demodulation analysis can obtain more useful information, it is applied to the reconstructed signal to extract the fault characteristic frequencies. Finally, simulation studies show the effectiveness of combining VMD and DCS in fault diagnosis, and the advantages of the proposed method are verified through experiments with rolling bearing inner race, outer race and compound faults.

Keywords: sparsity; DCS demodulation; rolling bearing; fault diagnosis; variational mode decomposition; VMD.

Reference to this paper should be made as follows: Zhen, D., Li, D., Feng, G., Zhang, H. and Gu, F. (2022) 'Rolling bearing fault diagnosis based on VMD reconstruction and DCS demodulation', *Int. J. Hydromechatronics*, Vol. 5, No. 3, pp.205–225.

Biographical notes: Dong Zhen received his Bachelor's and Master's degrees from Shandong University of Science and Technology in 2006 and 2009, and his PhD from the University of Huddersfield in 2012. Currently, he is a Professor and Doctoral Supervisor at Hebei University of Technology, mainly engaged in research on mechanical system fault diagnosis and condition monitoring, fault feature extraction and pattern recognition, mechanical system dynamics, etc.

Dongkai Li received his Bachelor's degree from Liaocheng University in 2020 and is currently a Master's student at Hebei University of Technology. His research direction is dynamic modelling and fault diagnosis methods of planetary gear transmission systems.

Guojin Feng received his Bachelor's and Master's degree from Shandong University of Science and Technology in 2009 and 2012, and PhD from the University of Huddersfield in 2016. Currently, he is a Lecturer and Master's Supervisor at Hebei University of Technology, mainly engaged in the research of intelligent condition monitoring system of rotating machinery and on-rotor MEMS sensing system, etc.

Hao Zhang is a Professor in the School of Mechanical Engineering at Hebei University of Technology. He is an experienced researcher in the fields of hydrodynamic lubrication, rotor-dynamics, mathematical modelling, modal analysis, etc. He is the author of 20 technical and professional publications in the relevant fields.

Fengshou Gu is a Professor of Machine Diagnostics at University of Huddersfield, and he is the Deputy Director of the Centre for Efficiency and Performance Engineering (CEPE) and the Head of Measurement and Data Analysis Research Group (MDARG) at CEPE. He has worked in the field of machine monitoring and diagnostic for more than 30 years in developing an advanced diagnostic laboratory and numerical simulation methods which have facilities to simulate various faults for majority machines. He is supervising over 40 PhD students and undertaking more than five contracts funded from UK and Chinese Government and industries.

This paper is a revised and expanded version of a paper entitled 'Rolling bearing fault diagnosis based on weighted variational mode decomposition and cyclic spectrum slice energy' presented at TEPEN 2021 & IncoME-VI, Tianjin China, 20th–23rd October 2021.

1 Introduction

As a support component, rolling bearings are widely used in various rotating machinery and equipment to ensure the proper rotation of the rotor (Laha, 2017). However, because rolling bearing are often subjected to heavy alternating loads (Dhamande and Chaudhari, 2018), the parts constituting the rolling element, such as inner ring, outer ring and rolling elements, are prone to pitting, peeling and other faults (An et al., 2016). Such faults of rolling bearing will reduce the performance of mechanical equipment, resulting in unnecessary downtime and maintenance cost (Li et al., 2017a). And the running state of the rolling bearing directly affects the proper operation of a machine (Li et al., 2021a). Monitoring its operating status, especially diagnosing its fault in time, is of great significance to the operation and maintenance of mechanical equipment (Yang et al., 2018).

Common rolling bearing fault diagnosis methods mainly include vibration analysis (Ding et al., 2018), acoustic signal analysis (Wang et al., 2021) and infrared analysis. Vibration analysis method is an effective method for condition monitoring and fault diagnosis of rotating machinery due to its characteristics of easy acquisition of vibration signal, high signal-to-noise ratio (SNR), cost-effective vibration sensor and wide application areas (Khadersab and Shivakumar, 2018).

Rolling bearing fault signal is nonlinear and non-stationary, its characteristics are often weak and easy to be submerged by interference components (Li et al., 2021b). These factors make it difficult to extract the features of rolling bearing. In recent years, based on vibration analysis, many scholars use time-frequency analysis methods to deal with fault signals. These methods include short-time Fourier transform (STFT) (Liu et al., 2020), wavelet transform (WT) (Zhang et al., 2021a), Wigner-Ville distribution (WVD), empirical mode decomposition (EMD) (Zheng and Pan, 2020) and so on. They have been successfully applied to fault signal analysis, but they also have limitations (Yan et al., 2018). For example, STFT cannot meet good time and frequency resolution at the same time. The decomposition effect of WT is closely related to the selection of wavelet basis (Hu et al., 2021). WVD has cross interference. Although EMD is adaptive, it has modal aliasing and endpoint effect (Li et al., 2017b).

To solve the above problems, variational mode decomposition (VMD), a new adaptive time-frequency analysis method, was proposed by Dragomiretskiy and Zosso (2014). VMD determines the central frequency and bandwidth of the modal component by iteratively searching the optimal solution of the variational model, decomposes the non-stationary signal into several intrinsic mode functions (IMFs), whose frequency bands are closely around the central frequency band. The essence of VMD is multiple adaptive Wiener filter groups, therefore, it has a solid theoretical basis and effectively avoids the modal aliasing and endpoint effect of EMD. The noise interference of VMD in the decomposition process is much less than that of EMD, and the influence of sampling effect can be suppressed by controlling the convergence condition. Due to its good performance, VMD has been widely used in the field of rotating machinery fault diagnosis in recent years. Wang et al. (2015b) compared and analysed the performance of VMD, EWT, EEMD and EMD in extracting features caused by rotor friction. Zhang et al. (2018) used grasshopper optimisation algorithm to improve VMD and solved the problem that its input parameters are difficult to determine. At present, most VMD algorithms use some indexes to select the optimal IMF for reconstruction, so as to reduce the influence of Gaussian noises.

For example, Dibaj et al. (2020) proposed the envelope spectrum weighted kurtosis index to select the sensitive mode. Xu et al. (2019) used the average kurtosis to select some IMFs whose kurtosis value is greater than the average kurtosis value to reconstruct the new signal. Yan et al. (2016) selected the IMFs containing the main fault feature information through the single failure feature amplitude energy ratio, and used it for subsequent analysis. Zhou et al. (2021) used the whale optimisation algorithm to determine the input parameters and reconstructed the modes greater than the average index. However, the information contained in other modal components is ignored when selecting the optimal mode reconstruction, which makes the reconstructed signal lack some detailed information contained in the original signal. Chen et al. (2009) used sparsity as an index to select effective components of EEMD, and explained the relationship between signal sparsity and energy. In view of the advantage of sparsity, this paper constructs a modal reconstruction coefficient by sparsity to measure the amount of useful information contained in different modal components, and all modes are reconstructed based on the reconstruction coefficient.

Because of the periodicity of the motion, the statistics of the early fault signals of rolling bearings are periodic time-varying and show cyclostationarity (Buzzoni et al., 2018). Cyclostationarity analysis is a powerful tool to deal with second-order cyclostationarity signal (Antoni, 2018). Wang et al. (2015b) used the cyclic spectrum slice energy to diagnose the bearing fault, and pointed out that it can make up the defect of envelope demodulation analysis. Antoni et al. (2017) proposed a new fast calculation method of spectral correlation based on STFT, which improved the calculation efficiency of spectral correlation. Kankar et al. (2013) fused cyclic autocorrelation with WT, and used support vector machine and artificial neural network to detect local defects of rolling bearing. Because cyclic autocorrelation is a two-dimensional function, it is relatively difficult and complex to extract useful information from it, so degree of cyclostationarity (DCS) is used to replace the cyclic autocorrelation function (CAF) for demodulation analysis. DCS represents the minimum distance between the autocorrelation function of non-stationary process and stationary process. It is a univariate function whose value range is between 0 and 1 with simple form (Antoni, 2009), and can fully express all the information of cyclic autocorrelation in the cyclic frequency domain. The modulation frequency can be extracted from the low frequency band of the DCS for the modulation signal, so as to obtain useful fault information and achieve the purpose of fault diagnosis. Chi et al. (2019) used DCS to diagnose the pseudo faults in rotor bearing system. Therefore, DCS demodulation is used to reveal the fault information contained in VMD reconstruction signal in this study.

To sum up, in order to solve the problem of heavy background noises and difficult extraction of fault features in rolling bearing fault diagnosis, this paper proposes a fault diagnosis method based on the combination of VMD reconstruction and DCS demodulation, which reduces noise interference through VMD reconstruction strategy and obtains the modulation information contained in fault signal by DCS demodulation, so as to extract fault features. There are two main innovations in this paper. Firstly, to avoid the loss of fault information caused by ignoring some IMFs in VMD, a weight coefficient calculation method based on sparsity is proposed to reconstruct all IMFs, which can highlight the sensitive IMFs and reduce interferences from other IMFs. Secondly, DCS is proposed to extract the fault characteristic frequency in the reconstructed signal by VMD while further suppressing the interference components. Its effectiveness is validated with experimental data by comparing with conventional envelope analysis and Teager energy operator (TEO). The rest of the article is organised as follows: Section 2 investigates theoretical background, Section 3 introduces the process of the proposed method, Section 4 and Section 5 verify the proposed method by simulation and experiment and the conclusions are drawn in Section 6.

2 Theoretical background

2.1 Variational mode decomposition

VMD (Jin et al., 2021) can adaptively decompose a complex signal into a series of IMFs, whose centre frequencies and bandwidths are determined by iteratively searching the optimal solution of the variational mode. In the frequency domain, IMFs are sparse, which can separate the intrinsic mode functions effectively.

The basic idea of VMD algorithm is to construct and solve the variational problem, decompose the complex signal into k IMFs. The constructed variational model can be described as follows:

$$\begin{cases} \min_{\{u_k\},\{\omega_k\}} \left\{ \sum_k \left\| \partial_t \left[\left(\delta(t) + j/\pi t \right) * u_k(t) \right] e^{-\mathrm{j}\omega_k t} \right\|_2^2 \right\} \\ \text{s.t.} \sum_k u_k = f \end{cases} \tag{1}$$

where ∂_t and (*) are partial derivative and convolution operations, u_k and ω_k represent the k^{th} IMF and its centre frequency, $\|\cdot\|_2$ is L_2 norm. To solve the above variational problem, the constrained variational problem is transformed into an unconstrained variational one by introducing the quadratic penalty factor and Lagrange operator. The augmented Lagrange function is:

$$\begin{aligned} L\left(\{u_k(t)\}, \{\omega_k(t)\}, \lambda\right) = \alpha \sum_{k=1}^{K} \left\| \partial_t \left[\left(\delta(t) + j/\pi t \right) * u_k(t) \right] e^{-j\omega_k t} \right\|_2^2 \\ + \left\| f(t) - \sum_{k=1}^{K} u_k(t) \right\|_2^2 + \left\langle \lambda, f(t) - \sum_{k=1}^{K} u_k(t) \right\rangle \end{aligned} \tag{2}$$

where α is the penalty factor, λ represents Lagrange operator; <·> means convolution. The alternating direction method of multipliers (ADMM) algorithm is used to solve the saddle point of the augmented Lagrange function. In this process, $\hat{u}_k^{n+1}$ and ω_k^{n+1} are updated by equation (3) and equation (4) respectively, so as to obtain the optimal solution of the variational problem.

$$\hat{u}_k^{n+1}(\omega) = \frac{\hat{f}(w) - \sum_{i \neq k} \hat{u}_i(\omega) + \hat{\lambda}(\omega)/2}{1 + 2\alpha(\omega - \omega_k)^2} \tag{3}$$

$$\omega_k^{n+1} = \frac{\int_0^\infty \omega \left| \hat{u}_k(\omega) \right|^2 d\omega}{\int_0^\infty \left| \hat{u}_k(\omega) \right|^2 d\omega} \tag{4}$$

2.2 *Reconstruction denoising strategy*

Most of the early faults of rolling bearing are localised pitting defects on the outer ring, inner ring and rolling elements. In the signal from faulty rolling bearing, the local pitting often appears as a periodic pulse, which makes the fault signal sparse. Sparsity (Miao et al., 2020) is a statistic that characterises the sparsity of time-domain signals. For a signal, the expression of sparsity is given in equation (5).

$$s = \left[\frac{1}{N} \sum_{n=1}^{N} x_i(n)^2 \right]^{1/2} \Bigg/ \left[\frac{1}{N} \sum_{n=1}^{N} \left| x_i(n) \right| \right] \tag{5}$$

When there are fewer Gaussian noise components and more impact components in signal, its power is concentrated in the pulse, and the amplitude has obvious multiple bulges. This signal shows strong sparsity. On the contrary, its power is dispersed into the interference components and the amplitude distribution of the signal is more uniform, so the sparsity is weaker. Therefore, this paper uses sparsity to construct the weight coefficients of each mode.

$$c(k) = s(k) \Big/ \sum_k s(k) \tag{6}$$

$$\hat{x}(n) = \sum_k c(k) u_k(n) \tag{7}$$

The signal is decomposed by VMD to get k IMFs, and the weight coefficient of IMF is defined as equation (6), where $s(k)$ represents the sparsity of the k^{th} IMF. Based on the sparsity of each IMF, the reconstruction coefficient is multiplied by each mode, and all processed modes are superimposed. The final expression of the weighted reconstructed noise reduction signal is shown in equation (7).

2.3 Degree of cyclostationarity

As a special case of non-stationary signal, the statistical characteristics of cyclostationary signals change periodically. According to different statistical characteristics of periodic cycle, they can be divided into first-order, second-order and high-order cyclostationary signals. And the second-order cyclostationary signal is a non-stationary signal whose autocorrelation function changes periodically.

The early fault signal of rolling bearing shows amplitude modulation characteristics. Its autocorrelation function is periodically time-varying and belongs to second-order cyclostationary signal. For it, equation (8) of time-varying autocorrelation function is obtained by the statistical average of the signal's time-delay quadratic transformation.

$$R_x(t, \tau) = E\left\{ x^*\left(t - \frac{\tau}{2}\right) x\left(t + \frac{\tau}{2}\right) \right\} \tag{8}$$

where E is mathematical expectation; (*) represents a conjugate operation. Since the time-varying autocorrelation function is a periodic function, it can be expanded by Fourier series as in equation (9).

$$R_x(t, \tau) = \sum_\alpha R_x^\alpha(\tau) e^{j2\pi\alpha t} \tag{9}$$

where $\alpha = n / T$ is the cycle frequency, which is related to the fault characteristic frequency. The cyclic spectral density (CSD) (Cheng et al., 2021) $R_x^\alpha(\tau)$ can be obtained by Fourier transform (FT) of CAF as follows:

$$S_x^\alpha(f) = \int_{-\infty}^{\infty} R_x^\alpha(\tau) e^{-j2\pi f\tau} d\tau \tag{10}$$

The CSD is a double spectrum diagram composed of cyclic frequency and spectrum frequency. In order to analyse the fault types of rolling bearings by using the cyclic frequency, the CSD is sliced along the direction perpendicular to the cycle frequency axis at each cycle frequency. And the DCS is defined as:

$$DCS(\alpha) = \frac{\int_{-\infty}^{+\infty} \left| S_x^{\alpha}(f) \right|^2 df}{\int_{-\infty}^{+\infty} \left| S_x^{0}(f) \right|^2 df} \tag{11}$$

3 Proposed algorithm

The fault signal of rolling bearing has the characteristics of low SNR, and its fault characteristics are easy to be submerged by complex interference components. To solve them, a fault diagnosis method using VMD reconstruction and DCS demodulation is proposed. The flowchart of the proposed algorithm is shown in Figure 1 and the operation details of this method are explained as follows:

Step 1 The non-stationary vibration signal is decomposed into a series of IMFs by VMD.

Step 2 The sparsity of each mode is calculated by equation (5), and the VMD reconstructed signal is obtained by equation (7).

Step 3 Based on the CSD, the reconstructed signal is demodulated by DCS shown in equation (11) to obtain more fault related information.

Step 4 Calculate the FFT of the signal and obtain the characteristic frequency of the fault signal.

Step 5 The characteristic frequency is compared with the theoretical fault frequency of rolling bearing to judge whether the rolling bearing has fault.

Figure 1 Flowchart of the method for extracting fault features of rolling bearing base on VMD reconstruction and DCS demodulation (see online version for colours)

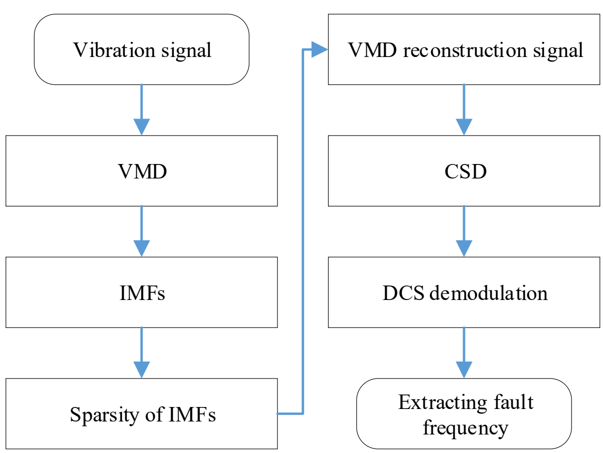

4 Simulation verification

When rolling bearing has a local pitting fault, there will be an impact on other parts in contact with the local pitting. With the rotation of the rolling bearing, the periodic pulse will be generated in the bearing fault signal, and there will be small sliding between the rolling element and the raceway. Therefore, a simulation signal from faulty rolling bearing is expressed as follows (Zhang and Shi, 2010):

$$\begin{cases} x(t) = \sum_i A_0 h(t - iT - \tau_i) + n(t) \\ h(t) = e^{-\beta t} \sin\left(2\pi f_n t\right) \end{cases} \tag{12}$$

where A_0 represents the amplitude and is set to 1, T denotes the interval of fault pulse, set to 1/70s, τ_i is the random slip caused by the i^{th} impact, it is related to T, β, represents the attenuation coefficient, equal to 800, f_s stands the sampling period, set to 10,000 Hz, t is the sampling time and is set to 1s, f_c denotes the bearing failure frequency, equal to 70 Hz, f_n stands the resonant frequency, set to 2,000 Hz. Considering that the rolling bearing works in harsh environment, Gaussian noise is added to the simulation signal and the SNR of the resulting signal is –7 dB.

Figure 2 Rolling bearing simulation signal, (a) raw signal (b) raw signal spectrum (c) noisy signal (d) noisy signal spectrum (see online version for colours)

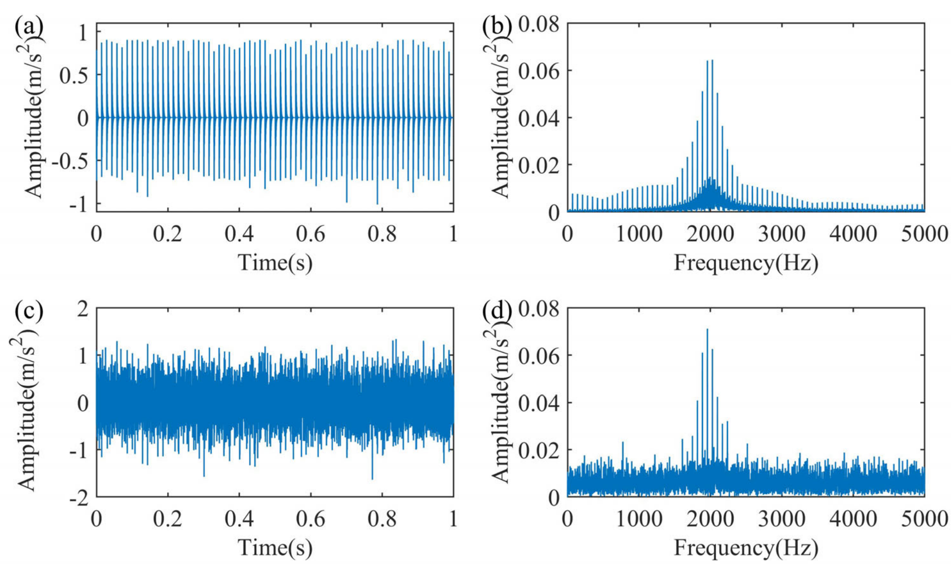

Figure 2(a) is a raw rolling bearing fault signal and Figure 2(c) shows the resulting signal after adding Gaussian white noise to it. In Figure 2(c), the regular periodic fault pulses are submerged by noises and there are many random shocks. The spectrum of the raw signal is shown in Figure 2(b). Figure 2(d) shows the spectrum with noise signal, in which the frequency components related to fault are submerged and are difficult to identify. It can be seen that the traditional signal analysis methods are invalid, so the diagnosis strategy proposed in this paper is applied to the simulated signal.

Firstly, VMD is applied to the simulation signal and modal reconstruction is carried out to suppress the noise. In this process, the number of modal components and penalty factor are closely related to its decomposition effect. The penalty factor of VMD determines the bandwidth of the modal component. When the penalty factor increases, the bandwidth of the mode decreases, on the contrary, the mode has a larger bandwidth. Zhang et al. (2021b) suggested that the penalty factor of VMD is 2,000, so the penalty factor in this paper is set as the same. If there are too few modal components, the decomposition is not complete. On the contrary, it will be over decomposed. Both of these situations will have an adverse impact on the decomposition effect, and they should be avoided as much as possible. In this paper, the central frequency method is used to determine the appropriate number of modes.

Figure 3 The results of the simulation signal decomposed by VMD (time-domain waveforms of IMF1-IMF7) (see online version for colours)

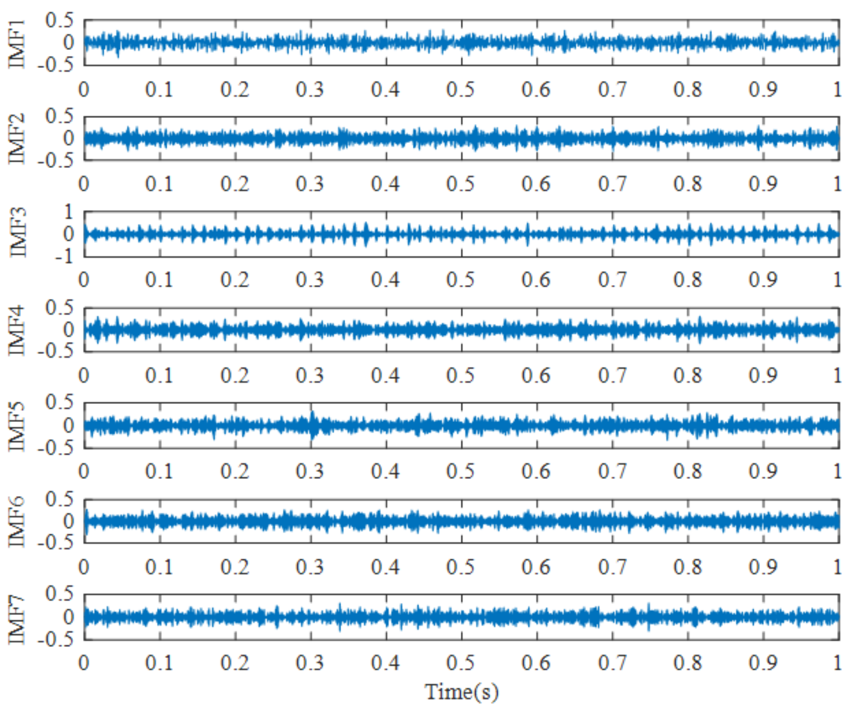

In this method, the number of IMFs is preset as 2, 3, …, 8, and the signal is decomposed to observe the centre frequency of adjacent IMF. Table 1 show the centre frequency difference of adjacent modes when the number of modes *k* takes different values. It can be found that when *k* is 6, the centre frequency between modal components 5 and 6 is too large, which is easy to cause incomplete decomposition. And if *k* is taken as 8, the centre frequency difference between modes 3 and 4 is 350 Hz, so over decomposition is easy to occur. Only when *k* is 7, the centre frequency of each mode is evenly distributed, so the VMD decomposition effect is the best. The number of modes is selected as 7 by using the centre frequency method and the decomposition results of VMD are shown in Figure 3.

Considering the amount of useful information contained in each IMF is different, all IMFs decomposed are reconstructed based on the modal reconstruction coefficient composed of signal sparsity. The expression of reconstructed signal is shown in equation (7). Figures 4(a) and 4(b) show the reconstruction coefficient of IMFs and the results of VMD reconstructed signal. Comparing the spectrum with noise signal, it can be found that some fault related frequencies in Figure 4(b), such as $3f_c$, $4f_c$, $5f_c$ and $6f_c$, have large amplitudes.

Table 1 The difference between the centre frequencies of adjacent modes when the number of modes k takes different values

k	u_{12}	u_{23}	u_{34}	u_{45}	u_{56}	u_{67}	u_{78}
2	1,183						
3	1,183	1,296					
4	1,032	420	2,036				
5	852	530	1,296	1,039			
6	753	735	559	840	1,004		
7	753	735	559	737	810	578	
8	538	833	350	559	737	810	578

Figure 4 Reconstruction coefficient of each mode and spectrum of VMD reconstructed signal, (a) reconstruction coefficients (b) reconstruction signal spectrum (see online version for colours)

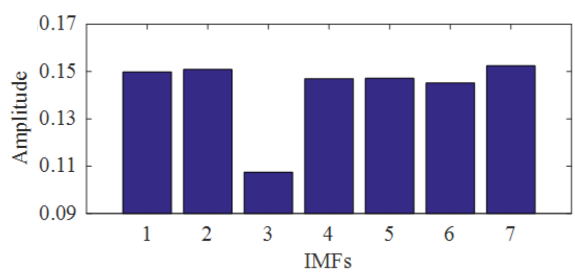

(a)

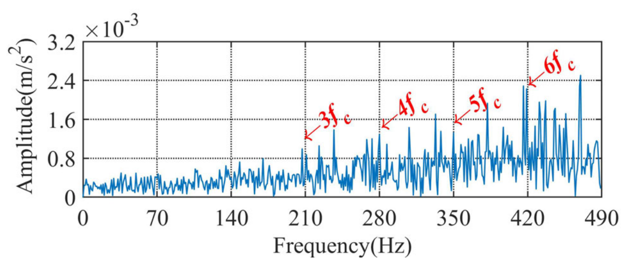

(b)

To illustrate the advantages of VMD reconstruction in noise reduction, two advanced signal denoising strategies are also used to process the simulation signal. Figure 5 is the root mean squared error (RMSE) and SNR indicators of the simulated signal after VMD reconstruction, EMD and WT threshold denoising. EMD selects the first two IMFs with the largest kurtosis for reconstruction, and the number of decomposition layers for wavelet threshold denoising is 3. When the denoising signal has a smaller RMSE and a larger SNR, the noise reduction effect is more significant. Figure 5 clearly shows that the proposed method has the smallest RMSE and the largest SNR, indicating that it has superior noise reduction performance.

To evaluate the denoising effect of the proposed method, noises with different levels are added to the raw signal and the resulting signals are processed by the proposed method respectively. Figure 6 shows that although the SNR of signal is very low, a higher SNR can be obtained after denoising by VMD. For example, for the simulated signal with SNR of –21 dB, the SNR after denoising can reach –3 dB.

Figure 5 RMSE and SNR of simulated signals processed by three different methods (VMD, EMD, and WT) (see online version for colours)

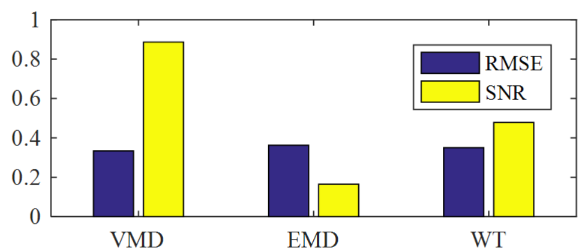

Figure 6 The SNRs of denoised signals obtained by VMD reconstruction strategy for simulated signals with different noises (see online version for colours)

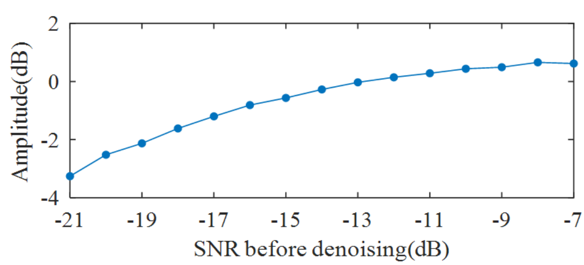

Note that the fault characteristics in the spectrum of VMD reconstructed signal are actually not obvious, which is easy to lead to misjudgment. Therefore, DCS demodulation is applied to the VMD denoising signal to extract the frequency characteristics of fault signal more clearly and ensure the accuracy of fault diagnosis. The CSD of the noise signal is calculated according to equation (10), and then the noise signal is demodulated by equation (11). The demodulation result of the reconstructed signal is shown in Figure 7, which can clearly display the fault characteristic frequency and its multiplication ($2f_c$, $3f_c$, …, $6f_c$). Through the DCS demodulation results, it can be judged that the bearing has outer ring fault, which is consistent with the fact.

Figure 7 The result of VMD reconstruction and DCS demodulation are applied to the simulation signal (see online version for colours)

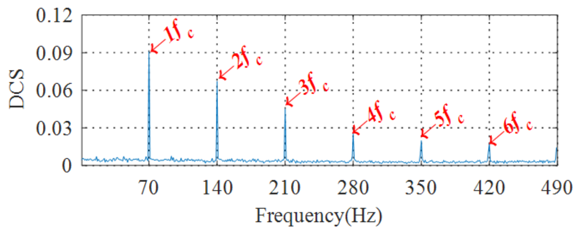

Figure 8 Test bench and fault parts, (a) rolling bearing test bench (b) rolling bearing outer ring fault (c) rolling bearing inner ring fault (see online version for colours)

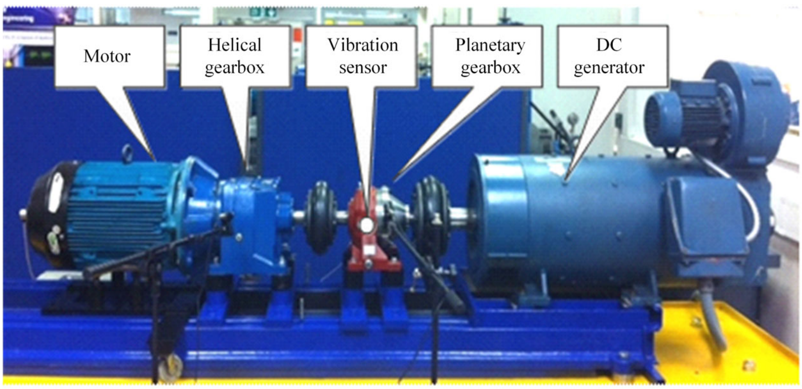

(a)

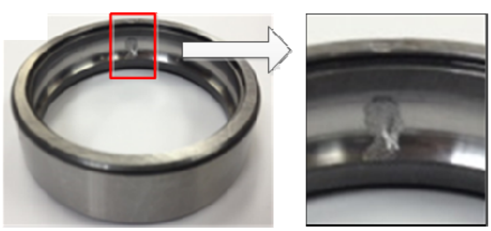

(b)

(c)

5 Experimental study

To further evaluate that the effectiveness of the proposed method for rolling bearing fault diagnosis, an experimental study is carried out. The rolling bearing test bench mainly includes an AC motor, a helical gearbox, a planetary gearbox and a DC generator, as shown in Figure 8(a). A vibration sensor is installed on the bearing seat of the drive end of the AC motor, and another one is mounted on the gearbox housing. The motor speed is set to 1,500 rpm. The length of bearing data collected in the test is 1,920,000, and the sampling frequency is 96 kHz. In this experiment, the types of bearing faults include motor bearing outer ring fault and planetary gear bearing inner ring fault. These two faults are manufactured artificially and picture of the faulty bearings are shown in Figures 8(b) and 8(c). The fault characteristic frequencies of motor bearing (6206ZZ) and planetary gear bearing (6008) are calculated and presented in Table 2.

Table 2 The fault characteristic frequencies of motor bearing and planetary gear bearing used in the experiment

Bearing model	*Inner ring fault (Hz)*	*Outer ring fault (Hz)*	*Roller fault (Hz)*	*Cage fault (Hz)*
6206ZZ	130.99	89.33	62.42	9.93
6008	65.17	49.25	33.60	4.10

5.1 Rolling bearing with outer ring fault

The time domain waveform and frequency spectrum of the rolling bearing with outer ring fault are shown in Figure 9. Due to interference of the background noise from the inside and outside of the equipment, the regular fault pulse cannot be found in the waveform of Figure 9(a), and the information related to the outer ring fault cannot be found in the spectrum of Figure 9(b). For diagnosing the fault of rolling bearing, the proposed diagnosis method based on VMD reconstruction and DCS demodulation is used to process the signal.

Figure 9 Test signal from rolling bearing with outer ring fault, (a) time domain waveform (b) frequency spectrum (see online version for colours)

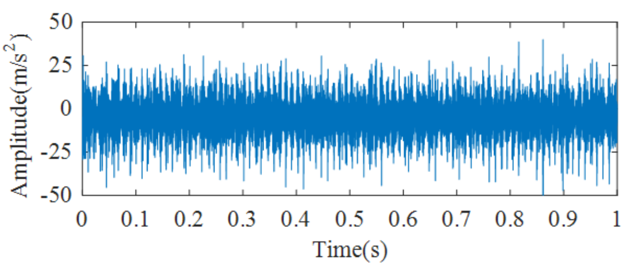

(a)

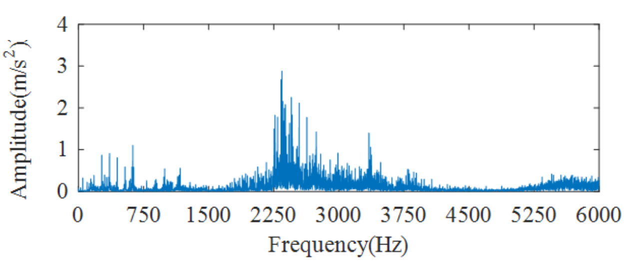

(b)

The experimental signal is firstly denoised by VMD. The number of modes is determined as 6 by the centre frequency method. In order to suppress noises, the reconstruction coefficient is calculated by equation (6) based on sparsity and the result is shown in Figure 10(a). The spectrum of the reconstructed signal is shown in Figure 10(b). Compared with Figure 9(b), the noise component in the figure is greatly reduced, especially the noise at low frequency is effectively suppressed, and partial harmonics of fault frequency, such as $3f_0$, $4f_0$, $5f_0$ and $6f_0$ are shown. However, the outer ring fault frequency and its second harmonic cannot be identified.

Envelope demodulation and TEO demodulation are two common demodulation methods. Figures 11(a), 11(b) and 11(c) show the results of applying envelope demodulation, TEO demodulation and DCS demodulation method on the reconstructed signal, respectively. Although the fault frequency and its harmonics can be identified in Figure 11(a), there exist some interference components. In Figure 11(b), only the first five harmonics of the fault frequency can be observed, and some unknown interference components can also be observed. In the meantime, Figure 11(c), which uses the proposed method, can clearly observe the spectral lines at the outer ring fault frequency and its harmonics. f_o and $2f_o$ are successfully recovered, and the interference components in the spectrum are effectively removed. According to the fault characteristic frequencies in Table 2, it shows that the motor bearing used in the experiment has outer ring fault, which is consistent with the fact. In summary, DCS demodulation can obtain more fault related information than the other two demodulation methods. Moreover, due to the white noise does not have cyclostationarity, the DCS demodulation based on cyclostationarity analysis can also effectively suppress the noise interference component.

Figure 10 (a) Reconstruction coefficient of each mode and spectrum of the VMD reconstructed signal (b) Spectrum of reconstructed signal (see online version for colours)

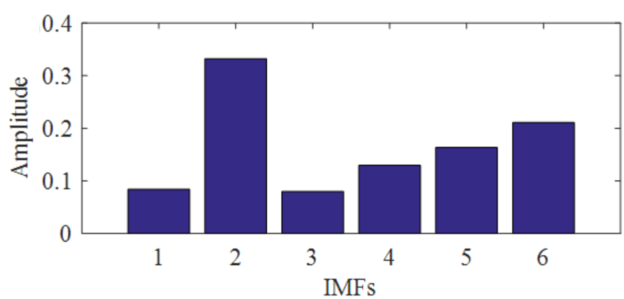

(a)

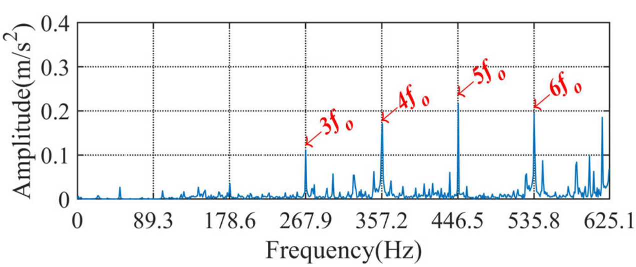

(b)

5.2 Rolling bearing with inner ring fault

To further validate the effectiveness of the proposed method for bearing fault diagnosis, it is applied to diagnose the signal from a planetary gear bearing with inner ring fault. Figure 12(a) shows its waveform, in which it can be seen that the pulses related to the inner ring fault are flooded by background noises and random shocks. Because the planetary gear bearing has complicated frequency components, the spectrum analysis shown in Figure 12(b) appears powerless and cannot extract the fault frequency component. Therefore, the method proposed in this paper is used to process the inner ring fault signal for feature extraction.

Figure 11 The reconstructed signal is demodulated by different methods, (a) envelope demodulation (b) TEO demodulation (c) DCS demodulation (see online version for colours)

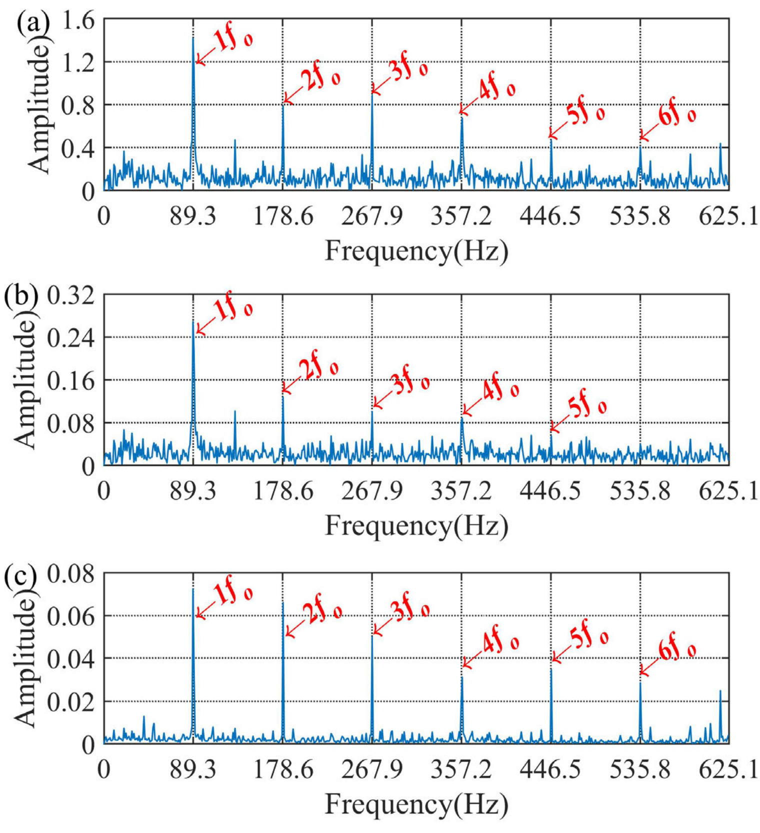

Figure 12 Vibration signal from an inner ring fault rolling bearing, (a) time domain waveform (b) frequency spectrum (see online version for colours)

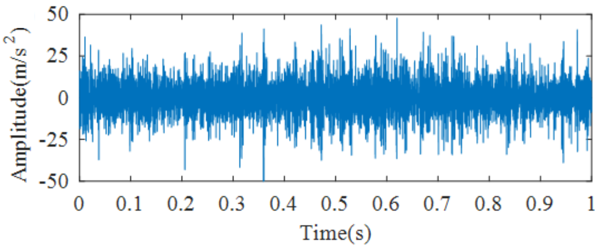

(a)

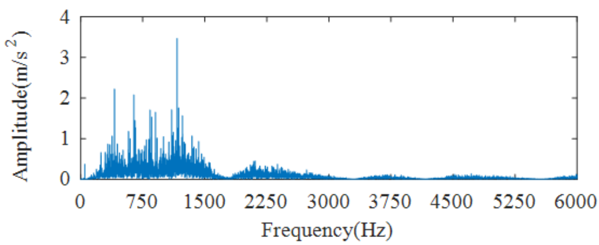

(b)

Figure 13 Reconstruction coefficient of each mode and spectrum of VMD reconstructed signal, (a) reconstruction coefficients (b) reconstructed signal spectrum (see online version for colours)

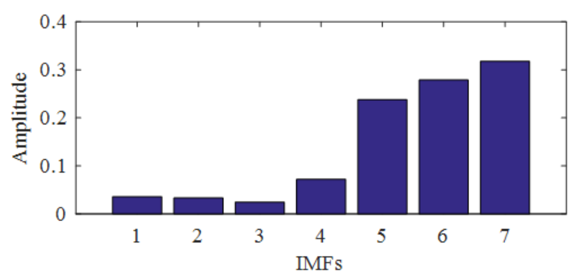

(a)

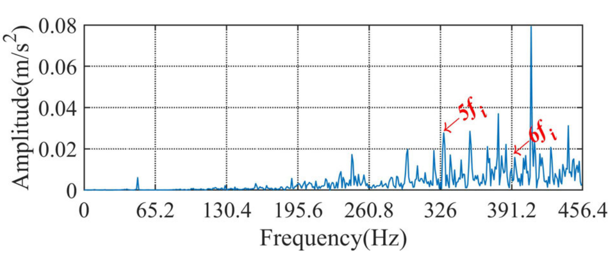

(b)

First of all, VMD reconstruction is applied on the signal to reduce noise. Figure 13(a) is the sparsity of the IMF after the fault signal is decomposed by VMD and Figure 13(b) shows the spectrum of VMD modal reconstruction based on the sparsity. It can be seen that the noise frequency is effectively suppressed, but fault characteristics still cannot be extracted yet. Next, DCS demodulation is applied to the reconstructed signal and the result is shown in Figure 14. In this figure, it can be found that the fault frequency and its harmonics ($2f_i$, $3f_i$, …, $6f_i$) have been successfully identified. The experiment of inner ring fault of planetary gear bearing further shows the advantages of combining VMD reconstruction and DCS demodulation.

Figure 14 The results of VMD reconstruction and DCS demodulation are applied to rolling bearing inner ring fault signal (see online version for colours)

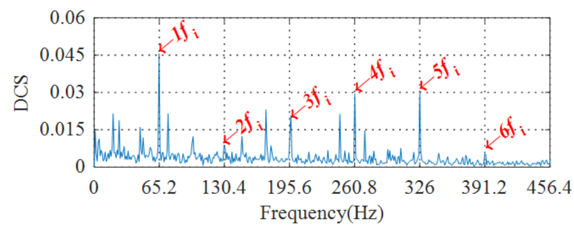

Figure 15 Vibration signal from a compound fault rolling bearing, (a) time domain waveform (b) frequency spectrum (see online version for colours)

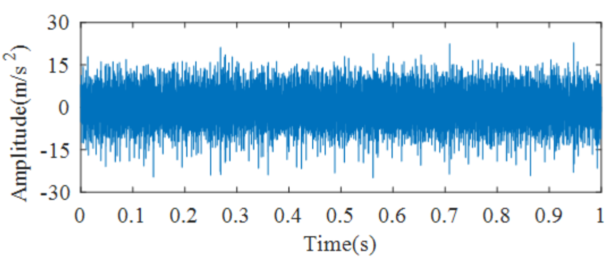

(a)

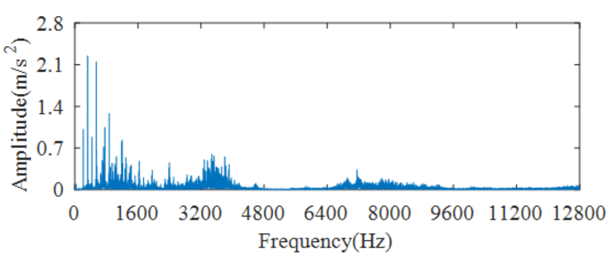

(b)

5.3 Rolling bearing with compound fault

In practice, a localised fault is likely to cause the evolvement of another type of fault, and hence multiple fault types may coexist on a rolling bearing. Such compound fault brings further challenges to the fault diagnosis. To further validate the effectiveness of the proposed method, it is applied to an accelerated life test dataset of rolling bearing from Paderborn University Bearing Data Center (Lessmeier et al., 2016). The 6,203 rolling bearing which contain a compound fault on inner and outer rings is used for analysis. The fault characteristic frequency of outer ring and inner ring (f_o and f_i) are 76.76 Hz and 123.24 Hz, respectively. Waveform and spectrum of the compound fault signal are shown in Figure 15. As can be seen, there are many pulses in the waveform and it is difficult to judge the fault type. The frequency components in the spectrum are complex and hence the fault type cannot be determined directly from the spectrum. Therefore, VMD-DCS method is used to analyse the signal.

Figure 16 The results of VMD reconstruction and DCS demodulation are applied to rolling bearing compound fault signal (see online version for colours)

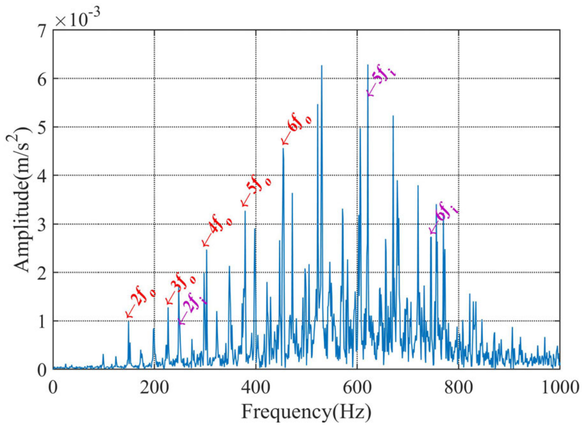

(a)

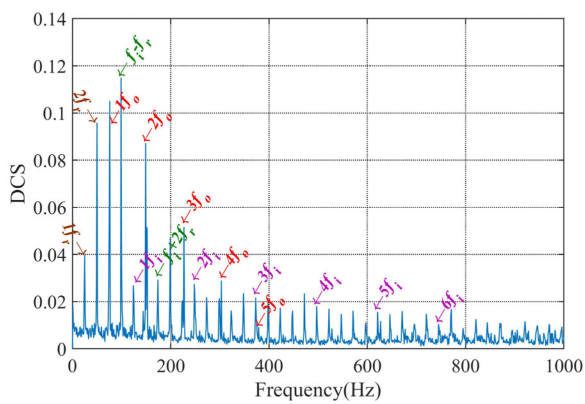

(b)

Figure 16(a) shows the spectrum of compound fault signal reconstructed by VMD, which are rather complicated. The frequency components related to inner and outer ring faults, for example $2f_o$~$6f_o$, $2f_i$, $5f_i$ and $6f_i$, can be identified. In order to judge the type of the bearing fault more clearly, DCS demodulation is applied to the reconstructed signal, as shown in Figure 16(b). The spectrum contains multiple frequency components but it is much easier to distinguish them in comparison with that in Figure 16(a). The significant frequency components include fault characteristic frequency and its harmonic components ($1f_o$~$5f_o$, $1f_i$~$6f_i$) of bearing inner and outer ring, modulation components ($f_i - f_r$, $f_i + 2f_r$) and rotating frequency f_r and its harmonics. This confirms the existence of compound fault on the inner ring and the outer ring of the bearing. The compound fault experiment again shows the superiority of the proposed method in suppressing background noises and extracting bearing fault related components.

6 Conclusions

Due to influence of background noise, the vibration signal acquired from rolling bearing can have low SNR, making it difficult to extract fault features. To address this problem, a diagnosis method combining VMD reconstruction and DCS demodulation is proposed in this paper, and the main conclusions are summarised as follows.

1. Sparsity can well measure the amount of fault information of the modes decomposed by VMD. Based on the reconstruction factor consisting of sparsity, reconstructed signal containing less background noise can be obtained. In the simulation study, the advantage of VMD reconstruction in suppressing interference components is shown compared with EMD denoising and WT threshold noise reduction.
2. By performing DCS demodulation on the VMD reconstructed signal, the rolling bearing fault characteristic frequencies can be clearly and accurately identified. It is proved that the demodulation capability of DCS is more powerful than envelope demodulation and TEO demodulation in that it can demodulate more information related to rolling bearing fault.
3. The effectiveness of the proposed method is demonstrated by evaluating it on simulation signals, and the advantages of combining VMD and DCS in fault diagnosis are verified by three experiments with planetary gear inner ring fault, motor bearing outer ring fault and rolling bearing compound fault.

References

An, X., Zeng, H. and Li, C. (2016) ‘Demodulation analysis based on adaptive local iterative filtering for bearing fault diagnosis’, *Measurement*, Vol. 94, pp.554–560.

Antoni, J. (2009) ‘Cyclostationarity by examples’, *Mechanical Systems and Signal Processing*, Vol. 23, No. 4, pp.987–1036.

Antoni, J. (2018) ‘Cyclic spectral analysis of rolling-element bearing signals: facts and fictions’, *Journal of Sound & Vibration*, Vol. 304, Nos. 3–5, pp.497–529.

Antoni, J., Xin, G. and Hamzaoui, N. (2017) ‘Fast computation of the spectral correlation’, *Mechanical Systems and Signal Processing*, Vol. 92, pp.248–277.

Buzzoni, M., Antoni, J. and D’Elia, G. (2018) ‘Blind deconvolution based on cyclostationarity maximization and its application to fault identification’, *Journal of Sound and Vibration*, Vol. 432, pp.569–601.

Chen, L., Li, X., Li, X. and Huang, Z. (2009) 'Signal extraction using ensemble empirical mode decomposition and sparsity in pipeline magnetic flux leakage nondestructive evaluation', *The Review of Scientific Instruments*, Vol. 80, No. 2, pp.1–6.

Cheng, Y., Chen, B. and Zhang, W. (2021) 'Enhanced spectral coherence and its application to bearing fault diagnosis', *Measurement*, Vol. 188, pp.1–17.

Chi, Y., Yang, S., Jiao, W., He, J., Gu, X. and Papatheou, E. (2019) 'Spectral DCS-based feature extraction method for rolling element bearing pseudo-fault in rotor-bearing system', *Measurement*, Vol. 132, pp.22–34.

Dhamande, L.S. and Chaudhari, M.B. (2018) 'Compound gear-bearing fault feature extraction using statistical features based on time-frequency method', *Measurement*, Vol. 125, pp.63–77.

Dibaj, A., Hassannejad, R., Ettefagh, M.M. and Ehghaghi, M.B. (2020) 'Incipient fault diagnosis of bearings based on parameter-optimized VMD and envelope spectrum weighted kurtosis index with a new sensitivity assessment threshold', *ISA Transactions*, Vol. 114, pp.413–433.

Ding, J., Zhao, W., Miao, B. and Lin, J. (2018) 'Adaptive sparse representation based on circular-structure dictionary learning and its application in wheelset-bearing fault detection', *Mechanical Systems and Signal Processing*, Vol. 111, pp.399–422.

Dragomiretskiy, K. and Zosso, D. (2014) 'Variational mode decomposition', *IEEE Trans Signal Process*, Vol. 62, No. 3, pp.531–544.

Hu, M., Wang, G., Ma, K., Cao, Z. and Yang, S. (2021) 'Bearing performance degradation assessment based on optimized EWT and CNN', *Measurement*, Vol. 172, pp.1–13.

Jin, Z., He, D., Ma, R., Zou, X., Chen, Y. and Shan, S. (2021) 'Fault diagnosis of train rotating parts based on multi-objective VMD optimization and ensemble learning', *Digital Signal Processing*, Vol. 121, pp.1–15.

Kankar, P.K., Sharma, S.C. and Harsha, S.P. (2013). 'Fault diagnosis of rolling element bearing using cyclic autocorrelation and wavelet transform', *Neurocomputing*, Vol. 110, pp.9–17.

Khadersab, A. and Shivakumar, S. (2018) 'Vibration analysis techniques for rotating machinery and its effect on bearing faults', *Procedia Manufacturing*, Vol. 20, pp.247–252.

Laha, S.K. (2017) 'Enhancement of fault diagnosis of rolling element bearing using maximum kurtosis fast nonlocal means denoising', *Measurement*, Vol. 100, pp.157–163.

Lessmeier, C., Kimotho, J., Zimmer, D. and Sextro, W. (2016) 'Condition monitoring of bearing damage in electromechanical drive systems by using motor current signals of electric motors: a benchmark data set for data-driven classification', *European Conference of the Prognostics and Health Management Society*, Vol. 3, No. 1, pp.5–8.

Li, J., Li, M. and Zhang, J. (2017a) 'Rolling bearing fault diagnosis based on time-delayed feedback monostable stochastic resonance and adaptive minimum entropy deconvolution', *Journal of Sound and Vibration*, Vol. 401, pp.139–151.

Li, P., Chen, J., Zi, Y. and Pan, J. (2017b) 'Independence-oriented VMD to identify fault feature for wheel set bearing fault diagnosis of high speed locomotive', *Mechanical Systems and Signal Processing*, Vol. 85, pp.512–529.

Li, W., Chen, J., Li, J. and Xia, K. (2021a) 'Derivative and enhanced discrete analytic wavelet algorithm for rolling bearing fault diagnosis', *Microprocessors and Microsystems*, Vol. 82, pp.1–8.

Li, J., Cheng, X., Li, Q. and Meng, Z. (2021b) 'Adaptive energy-constrained variational mode decomposition based on spectrum segmentation and its application in fault detection of rolling bearing', *Signal Processing*, Vol. 183, pp.1–17.

Liu, D., Cheng, W. and Wen, W. (2020) 'Rolling bearing fault diagnosis via STFT and improved instantaneous frequency estimation method', *Procedia Manufacturing*, Vol. 49, pp.166–172.

Miao, Y., Zhao, M., Hua, J. (2020) 'Research on sparsity indexes for fault diagnosis of rotating machinery', *Measurement*, Vol. 158, pp.1–13.

Wang, Y., Markert, R., Xiang, J. and Zheng, W. (2015a) 'Research on variational mode decomposition and its application in detecting rub-impact fault of the rotor system', *Mechanical Systems and Signal Processing*, Vols. 60–61, pp.243–251.

Wang, H., Chen, J. and Dong, G. (2015b) 'Fault diagnosis of rolling bearing based on spectral correlation density combined slice energy', *Journal of Vibration and Shock*, Vol. 34, No. 3, pp.114–117.

Wang, X., Mao, D. and Li, D. (2021) 'Bearing fault diagnosis based on vibro-acoustic data fusion and 1D-CNN network', *Measurement*, Vol. 173, pp.1–13.

Xu, B., Zhou, F., Li, H., Yan, B. and Liu, Y. (2019) 'Early fault feature extraction of bearings based on Teager energy operator and optimal VMD', *ISA Transactions*, Vol. 86, pp.249–265.

Yan, X., Jia, M., and Xiang, L. (2016) 'Compound fault diagnosis of rotating machinery based on OVMD and a 1.5-dimension envelope spectrum', *Measurement Science and Technology*, Vol. 27, No. 7, pp.1–17.

Yan, X., Jia, M., Zhang, W. and Zhu, L. (2018) 'Fault diagnosis of rolling element bearing using a new optimal scale morphology analysis method', *ISA Transactions*, Vol. 73, pp.165–180.

Yang, H., Lin, H. and Ding, K. (2018) 'Sliding window denoising k-singular value decomposition and its application on rolling bearing impact fault diagnosis', *Journal of Sound Vibration*, Vol. 421, pp.205–219.

Zhang, X., Miao, Q., Zhang, H. and Wang, L. (2018) 'A parameter-adaptive VMD method based on grasshopper optimization algorithm to analyze vibration signals from rotating machinery', *Mechanical Systems and Signal Processing*, Vol. 108, pp.58–72.

Zhang, Y. and Shi, L. (2010) 'Establishment and application of mathematical model for local fault of rolling bearing', *Journal of Vibration and Shock*, Vol. 29, No. 4, pp.73–76.

Zhang, K., Ma, C., Xu, Y., Chen, P. and Du, J. (2021a) 'Feature extraction method based on adaptive and concise empirical wavelet transform and its applications in bearing fault diagnosis', *Measurement*, Vol. 172, pp.1–15.

Zhang, Y., Ren, G., Wu, D. and Wang H. (2021b) 'Rolling bearing fault diagnosis utilizing variational mode decomposition based fractal dimension estimation method', *Measurement*, Vol. 181, pp.1–11.

Zheng, J. and Pan, H. (2020) 'Mean-optimized mode decomposition: an improved EMD approach for non-stationary signal processing', *ISA Transactions*, Vol. 106, pp.392–401.

Zhou, X., Li, Y, Jiang, L. and Zhou, L. (2021) 'Fault feature extraction for rolling bearings based on parameter-adaptive variational mode decomposition and multi-point optimal minimum entropy deconvolution', *Measurement*, Vol. 173, pp.1–16.